crystals

MDPI

*Article*

# Graphene Based FET Biosensor for Organic-Phosphorous Sample Detection and the Enzymatic Analysis

**Jieyi Zhu [1,*], Meiyan Feng [2] and Guofu Lian [2]**

[1] School of Electronic, Electrical Engineering and Physics, Fujian University of Technology, Fuzhou 350108, China
[2] School of Mechanical and Automotive Engineering, Fujian University of Technology, Fuzhou 350108, China
* Correspondence: zhujieyi@mail.ustc.edu.cn

**Abstract:** Our paper presents a flexible enzymatic acetylcholinesterase graphene based FET biosensor of the target organic phosphorous. The sensor's purpose is to detect pesticide residues in the field of food safety. In our sensor design, the material is graphene with its functionalization, and graphene based FET structure will be discussed in one section of this paper. The mechanism of this graphene sensor is the enzymatic linked reaction on a sensor surface. The enzyme is fixed on the sensor surface by the linker 3-mercapto propionic acid. Measurement experiments using the biosensor were performed for detecting the concentration of isocarbophos (an organophosphate). The enzymatic biosensor has successfully detected 100 μg/mL isocarbophos from the water sample, presenting a significant detection limit index for organophosphate detection.

**Keywords:** graphene; enzymatic sensor; organophosphate detection



**Citation:** Zhu, J.; Feng, M.; Lian, G. Graphene Based FET Biosensor for Organic-Phosphorous Sample Detection and the Enzymatic Analysis. *Crystals* **2022**, *12*, 1327. https://doi.org/10.3390/cryst12101327

Academic Editors: Tomasz Tański, John Parthenios and Abdullah Mohamed Asiri

Received: 4 August 2022
Accepted: 16 September 2022
Published: 20 September 2022



## 1. Introduction

In China's agriculture food safety field, many traditional pesticide residue sensors have been developed and used over decades. However, the defects and deficiencies of traditional sensors lead to research on and applications of new materials for sensor development. The purpose of this paper is to present a graphene-based biosensor to detect organophosphorus within pesticide residues. The design of micro biosensors consists of sensor surface design, structures and mechanism. For sensor design, specific sensing material would be placed on the sensor surface by the graphene transfer process; this material would present a specific sensing mechanism. For instance, graphene-based sensors have been fabricated for detecting hydrogen peroxide as reported in J. S. Kumar's paper [1]. Furthermore, other substances could become sensor materials, such as magnetic materials and ferromagnetic materials [2]. For example, two dimensional transition metal di-chalcogenides (TMDC) are becoming promising [3]. Compared to TMDC material, graphene has biocompatibility properties as the sensing material has oxide linking chemical groups. Graphene is a zero-gap semiconductor to some general material [4,5]. Graphene has been used as the bio-function sensor material for some specific chemical detection tasks due to its excellent electrical and biocompatibility performance [6]. In recent years many research groups have utilized graphene as sensor detectors [7]. Although there are some limitations and deficiencies [8], graphene based FET sensors have also been used on many different occasions [9]. In recent research, Labchinskii's group used graphene-based on-chip multisensory arrays, utilizing the synthesis technology to develop gas sensors for detecting various vapors [10]. Furthermore, in Chen's paper graphene oxide was used to develop a surface plasma resonator biosensor [11]. Graphene thiolation technology was also used in reduced graphene oxide for enhanced photodetection [12].

The detection mechanism of the enzymatic biosensor is that the organophosphorus pesticides would inhibit the enzyme acetylcholinesterase (AChE) [13]. The traditional detection methods, including spectrophotometry [14], spectrofluorimetry [15], quartz

crystal microbalance [16] and so on [17], have their own disadvantages. These include long analysis time and expensive detection cost. In contrast, the indirect flexible enzymatic biosensor could successfully bring a rapid and cheap detection method. Furthermore, a high quality micro biosensor would allow repeated detection of the organophosphorus pesticides samples, providing excellent sensitivity and selectivity.

Isocarbophos is an organophosphate which has been widely used during the spread of insecticides. It is mainly used to control cotton spider, cotton aphid, cotton bollworm (larva and egg), red bollworm egg, spodoptera litura, and rice borer, and has a good effect on all kinds of scale insects. In 2022, there have been research papers about micro sensors for the rapid detection of organophosphate by some advanced means, such as electrochemical and fluorescence methods [18,19]. In our research, a graphene based organophosphate sensor could also have significant sensitivity and selectivity for rapid detection of organophosphorus pesticides. For sensor signal measurement experiments, the instrument we used is source meter Keithley 4200A-SCS, and we updated its software for sensor data processing. This Keithley instrument is developed by the Tektronix company; the 4200A-SCS is an industry-leading electrical characteristic parameter analyzer, providing synchronous current voltage curve test (I−V curves measurement) and other electrical signal measurement.

## 2. Sensor Design

In this biosensor design, after adequate research we chose the model solution gate field-effect transistor (FET) sensor; the sensing material is graphene. In order to detect the target organophosphorus sample, the graphene surface needs to be processed by a special functionalization protocol. The sensor bottom is p doped $Si/SiO_2$ substrate; the substrate's bottom side is Si, and the upper side is $SiO_2$. The oxide layer thickness is 100 nm. The Au electrode was chosen for its excellent electrical performance; the two gold electrodes were finished by a metal deposition process. The graphene size is 1.1 mm × 0.6 mm; during the fabrication process we would place this graphene nanoribbon across the two electrodes by graphene transfer protocol. In order to form the experiment chamber, we selected the material silicone rubber, and let the silicone rubber surrounding the graphene nanoribbon. For measurement, we need to apply the $V_{DS}$ between source and drain electrodes, and the sensor chip would be fixed on the probe station surface.

There are several kinds of FET, such as back-gate FET and solution gate FET. In our experiment, because our target sample is liquid, so we designed a solution gate FET sensor. During the experiment process, the sensor chip was fixed on the probe station surface, and the third needle of this probe station would touch the solution area to apply the gate voltage. The source-drain bias and source-gate bias share common grounding for safety reasons, which is the common practice of sensor design and electrical circuit design. The overall design of our biosensor is shown in Figure 1.

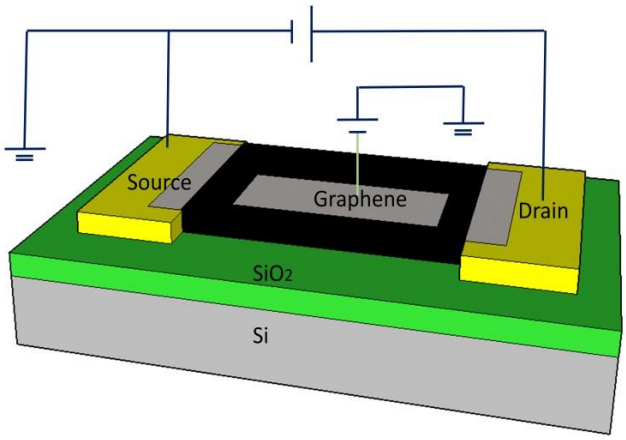


**Figure 1.** The schematic figures of our FET biosensor design. The detection target is an organophosphorus sample; the periphery circuit helps to conduct the measurement.

## 3. Fabrication and Functionalization

### *3.1. Fabrication of the Biosensor*

After the sensor design, we need to process the fabrication and functionalization. At the beginning the fabrication protocol needs to be processed. For the first step of fabrication, we need to finish the fabrication of the substrate with electrodes. After we obtained the $Si/SiO_2$ substrate, this substrate was cleaned in acetone, alcohol, IPA and DI water consecutively. It was then placed in plasma cleaner for 10 min. Later, we conducted the process with the spin-coater; the photoresist was spin coated on the substrate $SiO_2$ side. Next, the sensor chip was placed on a hotplate for prebake, under the temperature 110 °C for 10 min. In order to form the electrode pattern on the $SiO_2$ side of the substrate, a photolithography process was conducted with our designed photomask. The next step is metal deposition: the two electrodes are deposited on the $SiO_2$ side of the substrate, the electrode material is chosen as Cr/Au, the gold electrode's thickness is 100 nm, while the thickness of Cr is 15 nm for the Cr/Au electrode. The metal deposition process was conducted by Q150 TS in our laboratory. For the second step of fabrication, we needed to process graphene direct transfer. We placed one layer of PMMA on the Cu side of the graphene/Cu sheet, 30 min for drying. Next, the graphene sheet was placed into $FeCl_3$ aqueous solution at room temperature in order to etch the Cu layer. For about 10 h, the Cu material detached from the former graphene sheet, and what we obtained was PMMA/graphene. After this step we placed the PMMA/graphene sheet onto the substrate's $SiO_2$ side. Then the chip was under post bake at 80 °C for 5 min, and the post bake was at 150 °C for 15 min. Lastly, acetone is used to wash away the PMMA layer. For the third step of fabrication, we needed to transfer the finished graphene on the spare chip to the experimental chip. Finally, we therefor adjusted the graphene nanoribbon at an appropriate position and angle on the center of the substrate, as the graphene across the source electrode and drain electrode. The fabrication process and the pattern of this graphene sensor are shown in the Figure 2.

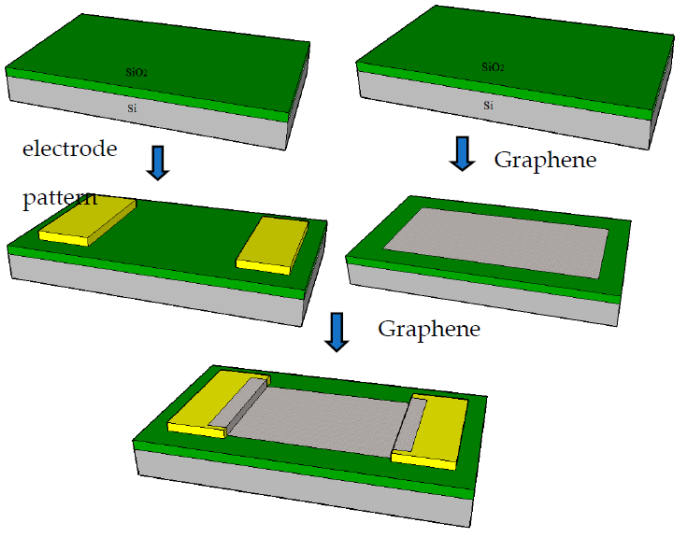


(**a**) The photolithography steps of sensor fabrication.

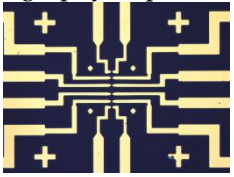

(**b**) The pattern for source and drain electrode pairs.

**Figure 2.** The schematic figures for the fabrication steps of the biosensor. (**a**) The sensor surface material had been processed in two photolithography process. (**b**) The fabrication of gold electrodes was according to the designed pattern.

### *3.2. Functionalization of the Biosensor*

For the first step of functionalization, 25:75 (v:v) water/ethanol solution within 70 mM MPA was dripped onto the sensor sensitive area for about 9 h, in order to establish the Au-MPA SAM. Then the chip was washed thoroughly by the 1:3 ethanolic solution and dried by $N_2$ gas. For the second step of functionalization, EDC/NHS activation was conducted to activate the NHS. This solution was dropped onto the gold gate surface and left for 4 h. For the third step of functionalization, the samples were again thoroughly washed by PBS buffer, after which we immediately dropped 50 µL of 2 mg/mL AChE on the FET's gate area which had been activated. For the fourth step of functionalization, we kept the samples for drying at room temperature for around 12 h, in order to let the liquid evaporate. When the functionalization steps were finished, the samples were washed by PBS buffer and stored at 4 °C in the laboratory refrigerator. The functionalization was performed on the entire sensor surface, after which the active graphene area would be surrounded by silicone rubber. The functionalization sequence is shown in the Figure 3.

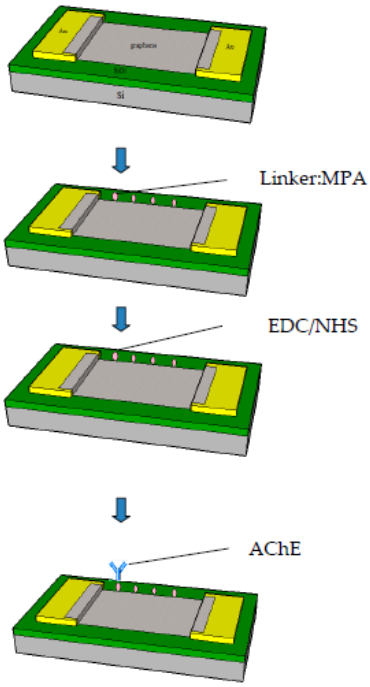


**Figure 3.** The linker is 3-Mercaptopropionic Acid(3-MPA), the enzymatic complex is acetylcholinesterase (AChE).

## 4. Experiment and Data

### *4.1. Experimental Setup*

After fabrication and functionalization, the sensor chip was fixed on the center of the probe station by magnetic force. As shown in Figure 4, the left needle and the right needle contact source and drain electrodes, providing source meter Keithley 4200A's bias voltage. For measurement, we conducted the control experiment and the target organic phosphorous experiment, respectively. In the control experiment, we added PBS, while we added isocarbophos solution for the target phosphorous detection experiment. For both the control experiment and the target phosphorous detection experiment, the bias voltage $V_{ds}$ was scanned from $-0.1$ V to 0.1 V for I−V curve measurement. The solution gate FET was chosen for the measurement, and the PBS solution and the target organic phosphorous solution were added into the recording chamber of the sensor. For transfer curve measurement, the gate voltage $V_g$ was scanned from 0 V to 0.8 V. The measurement instrument Keithley 4200-SCS is famous for its excellent parameter analysis performance, and the EPS-300 probe station also provides the optimal experiment conditions for our measurement. The figure of the experiment is shown in Figure 4.

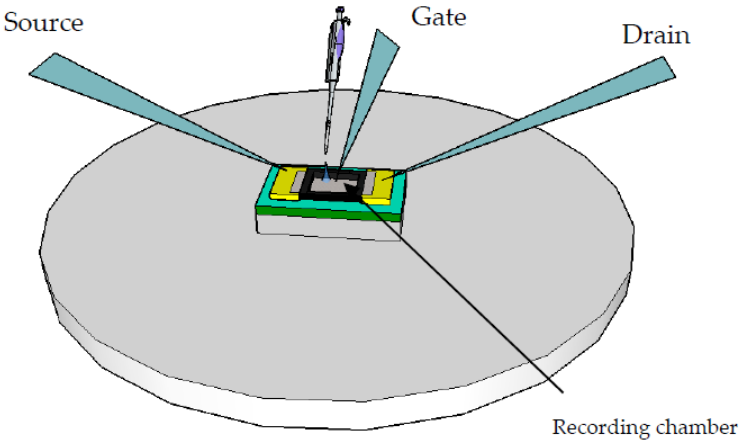


**Figure 4.** The schematic figure for the probe station with its three needles, contacting the source electrode, the drain electrode and the gate of the FET sensor, respectively.

For data collection and data processing, we used the source meter Keithley 4200A and its software. During the experiment, the source meter recorded two channels' sensor signal.

Before the measurements, we needed to culture the pesticide residue organic phosphorous. Organic phosphorous was purchased from Guangdong lab. In our experiment, we set $V_g$ = 0 V, and $V_{DS}$ = 0.1 V. The target organophosphate isocarbophos's chemical formula is $C_{11}H_{16}NO_4PS$, and its molecular mass is 289.29. The relationship between isocarbophos and the enzyme AChE is inhibition [20]. For the gold electrode, the linker MPA's alkane thiol group is prone to form a self-assembly monolayer due to its high affinity to gold [21]. After the ordered monolayers of alkane thiol group form, this linker could be used to immobilize the enzyme [22]. In our experiment, we planned to use the enzyme AChE on the gold electrode surface of the graphene-based FET sensor.

### *4.2. Sensor Surface Characterization*

In order to present and study the sensor material's performance, we conducted Raman spectrum and atomic force microscopy (AFM) scanning for this biosensor. The Raman spectra of graphene on the electrode area, and on the silicone substrate area are shown in Figures 5 and 6, respectively. Usually the graphene Raman spectrum has two peaks. The left peak is the G peak, and the right peak is the 2D peak. In our graphene Raman spectrum, the G peak is about 1583.41/cm$^2$, and the 2D peak is about 2705.71/cm$^2$. The multi-layers graphene would have different Raman spectrum peaks compared with single-layer graphene; when the layers increase the G peak would decrease, while the 2D peak would increase. The Raman spectrum peaks have been explained recently by the spectrum analyses in references [23,24].

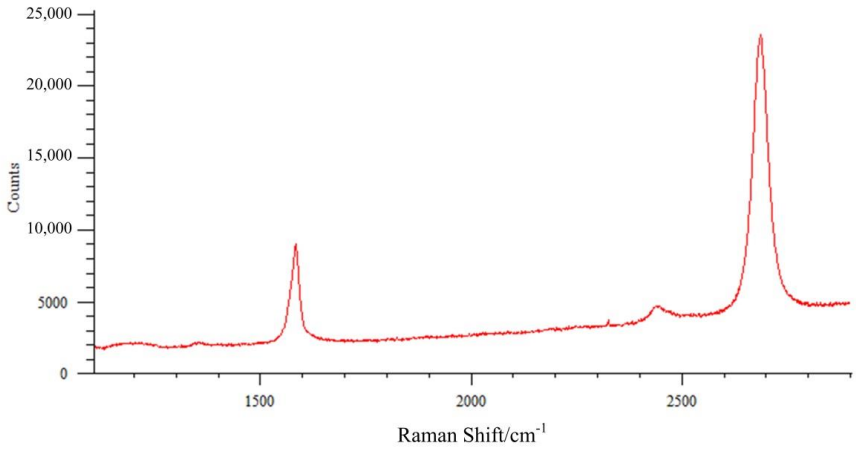


**Figure 5.** The graphene's Raman spectrum on the electrode area.

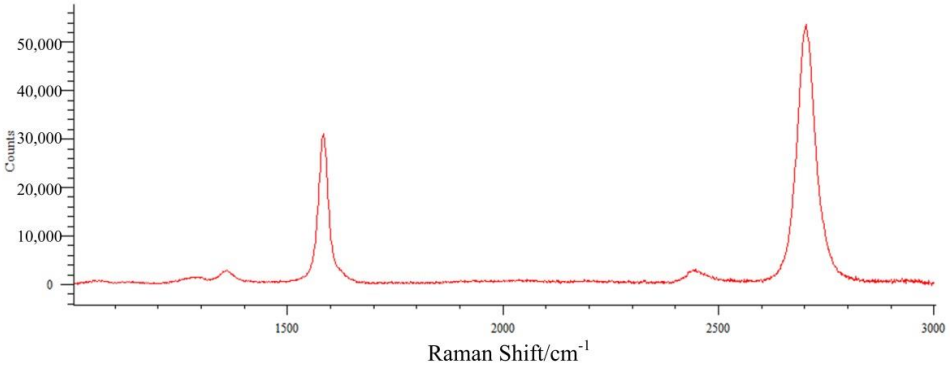


**Figure 6.** The graphene's Raman spectrum on the silicone substrate area.

From the Raman spectrum we could see that in our experiment the graphene was mainly two-layer graphene. Additionally, the defect peak of graphene was weak in the gold electrode area and silicone substrate area, indicating that the experimental graphene had few defects. The second characterization we undertook was AFM scanning. AFM stands for Atomic Force Microscope; this can detect the physical properties, including morphology, from regions of various materials and samples in the atmosphere and liquid environment. For AFM characterization, there are three working modes during this process, includingthe non-contact mode, the contact mode and the tapping mode. During the characterization process, the AFM instrument was in tapping mode. The AFM characterization image recorded is shown in Figure 7:

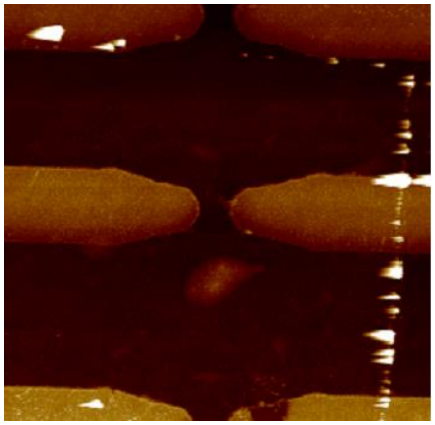

(**a**) The AFM characterization of sensor surface's inactive area between one pair of electrodes.

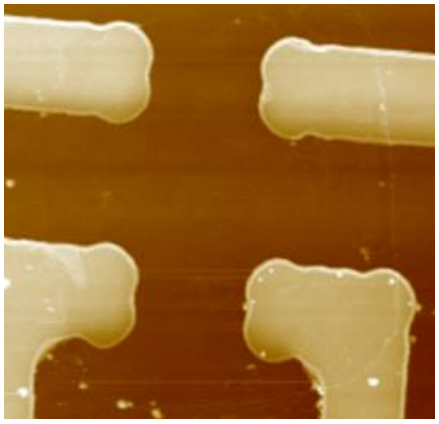

(**b**) The AFM characterization of sensor surface's active area before graphene transfer process between the source and drain electrode.

**Figure 7.** *Cont*.

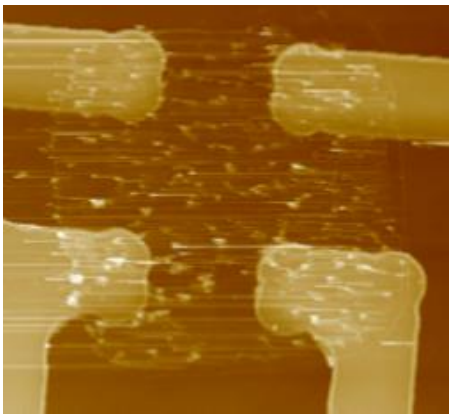

(**c**) The AFM characterization of sensor surface's active area after graphene transfer process and functionalization between the source and drain electrode.

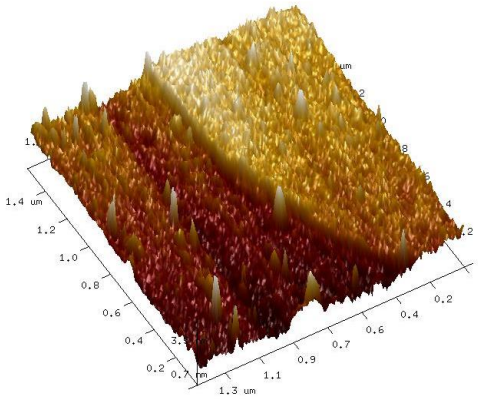


(d) The Section 3D figure of sensor surface's active area for AFM characterization

**Figure 7.** The AFM characterization figure of the sensor surface during the experiment process. (**a**) is the AFM characterization for sensor surface's inactive area without graphene, (**b**) is the AFM characterization for sensor surface's active area before graphene transfer, (**c**) is the AFM characterization for sensor surface's active area after graphene transfer, (**d**) is the Section 3D figure for AFM characterization with size and scale (size: 1.4 × 1.4 μm, scale: one line segment represents 0.2 μm).

In summary, from the AFM characterization we could observe the sensor surface's condition for both graphene and electrodes, and we could also observe the surface morphology by AFM's special features. The entire sensor chip size was 1 cm × 1 cm during the characterization and the following measurement, while the electrode width was about 1 mm (Figure 7b,c). Figure 7b shows the sensor surface's active area before the graphene transfer process, while Figure 7c shows the sensor surface's active area after the graphene transfer process. Figure 7a shows the sensor surface's inactive area. Figure 7d was collected from the borderline area between the graphene nanoribbon and electrode. The scansize is 1.4 × 1.4 μm, and the scale is that one line segment represents 0.2 μm. Compared to electron microscopy, AFM could be able to represent the surface morphology of this sensor, displaying the three-dimensional perspectives of the graphene sensor surface.

## 5. Sensor Signal Analysis

When we conducted the sensor experiment, the theoretical analysis was also undertaken to explain our results. From a theoretical point of view, the ideal graphene is considered without doping. However, in reality, the actual graphene has different degrees of doping level. In our experiment, the copper-based CVD graphene we used presented as p-doped even under $V_g$ = 0 V. For the FET sensor, the gate voltage could be used to adjust the doping level via field effect. The source meter Keithley 4200A could help us record the I−V curves and transfer curves; by observing the curves we could find there are

differences between experimental curves and theoretical curves. There have been some previous research papers about adjusting the doping level [25]. There are some relationships between the carrier density and doping level; in this case the equation about carrier density is utilised, as shown in Equation (1):

$$n = \sqrt{n_0^2 + (C_{OX}(V_g - V_D)/e)^2} \tag{1}$$

For theoretical analysis, the I−V curves and C−V curves could be deduced with their inherent relationship from the Landauer formula [26]. Later in Meric's paper, the actual curve was compared with the theoretical curve by mathematical deduction, considering some important parameters in the equation below:

$$I_d = \frac{W}{L}\int_0^L en(x)v_{drift}(x)dx \tag{2}$$

The reference paper constructed the compact mathematical model for this biosensor [27]. Furthermore, Petrone undertook theoretical analysis to strengthen this mathematical model [28]. Combining those references, the I−V relationship could be shown in the equation below:

$$I_{DS} = e\frac{W}{L}\mu_{eff}n_oV_{ds} \tag{3}$$

$$I_{DS} = \frac{\frac{W}{2L}e\mu_{eff}(-C_{ox}(V_g - V_D)/e + \sqrt{n_0^2 + (C_{ox}(V_g - V_D)/e)^2})V_{ds}}{1 + \frac{\mu_{eff}V_{ds}}{Lv_{sat}}} \tag{4}$$

After adding the target solution, the realistic I−V relationship could be as presented in Equation (5):

$$I'_{DS} = e\frac{W}{L}\mu_{eff}(n_0 + \frac{V_I}{V_T}\cdot c\cdot\frac{\rho_0 k_T}{\rho_0 k_T + 1}\cdot Q_E)V_{ds} + \Delta I_d \tag{5}$$

In these equations, Equation (3) describes this sensor's I−V performance under Vg = 0 V for both the control experiment and the target detection experiment; Equation (5) presents the transfer curves under specific circumstances when we set a gate voltage $V_g$ together with the fixed $V_{ds}$. In the above equations, W and L stand for channel width and length respectively, $\mu_{eff}$ is the effective carrier mobility, $n_0$ is the initial carrier density under $V_g$ = 0 V situation, $V_g$ is gate voltage, $V_D$ is threshold voltage at Dirac point, $V_{ds}$ is bias voltage. When we consider C−V curves, the gate capacitance would be considered. $C_{ox}$ stands for the oxidation layer gate capacitance, c stands for the organophosphorus solution concentration.

In our experiment, the measurement instrument Keithley 4200A source meter recorded the I−V curves and transfer curves for the control experiment and the target detection experiment. When we set $V_g$ = 0 V, the I−V curves would be obtained from the source meter. In this experiment, we did not focus on transfer curves, which were obtained from the condition that when we set a gate voltage $V_g$ together with the fixed $V_{ds}$. For the I−V curves recording process, the parameters were set as follows: the bias voltage $V_{ds}$ = 0.1 V, the gate voltage $V_g$ = 0 V. For transfer curves measurement, we set the bias voltage $V_{ds}$ = 0.1 V, while $V_g$ ranged from −0.8 V to 0.8 V. The prepared isocarbophos sample was obtained from the China National Analytical Centre (NACC), Guangzhou. The concentration of the isocarbophos sample was about 100 µg/mL. The reference paper about the Landauer theoretical model suggested the conditions for monolayer graphene [29]. For multilayer graphene and actual graphene surface, the surface chemical groups should be considered in the theoretical analytical model, such as sulfhydryl and hydroxyl groups.

The above Figure 8 demonstrates the result of the sensor for sensing the neurotransmitter acetylcholine. After adding the AChE, there was an obvious increase in the drain-to-source current. After AChE hydrolysis reaction, the reaction products included choline and

acetic acid, releasing $H^+$ ions into the electrolyte, producing $H_2O$. The ACh's hydrolysis process could be presented in the chemical Equation (6) below:

$$\begin{gathered} CH_3COO(CH_2)_2N^+(CH_3)_3 + H_2O \overset{AChE}{\rightarrow} (CH_3)_3(CH_2)_2NOH + CH_3COOH + H^+ \\ CH_3COOH \rightleftarrows CH_3COO^- + H^+ \end{gathered} \quad (6)$$

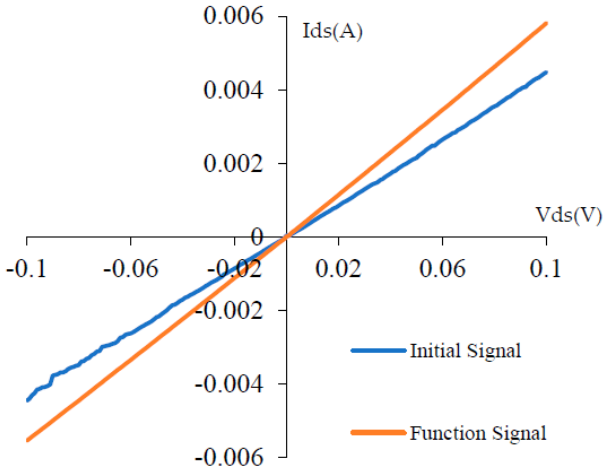


**Figure 8.** I−V curves corresponding to the initial signal, and the signal after thiolation, AChE functionalization.

The above chemical equations are a pair of combination equations, which happen concurrently in the sensor's chamber. For this pair reaction, the decomposition reaction of acetic acid is a reversible reaction. The AChE becomes the catalytic agent of the hydrolysis process. During the experiment, after adding the ACh, the enzyme AChE leads to the catalytic reaction [30]. The enzyme concentration would affect the tendency of the chemical equilibrium, being regarded as the catalyzer of the reaction. The $H^+$ ions released on the sensor surface caused the potential change [31].

This kind of biosensor is firstly used as a neurotransmitter acetylcholine sensor [32]. Solutions of the organophosphate isocarbophos were prepared in the solvent of PBS buffer, at a concentration of 1 mM. For the control experiment, the bias current was measured with a 1 nM acetylcholine concentration without the target isocarbophos, and was recorded as $V_{ds,control}$. After the target organic phosphorous isocarbophos was attached the solution was well mixed for some time about 5 min. Then the drain-to-source current was recorded as Ids. We calculated the inhibition of the enzyme activity from the difference of these two drain-to-source current values [33]. The inhibition equation is shown in Equation (7):

$$\text{Inhibition}\% = \frac{I_{ds,control} - I_{ds}}{I_{ds,control}} \times 100\% \quad (7)$$

In the above formula, $I_{ds}$ stands for the current measured in in 1 nM acetylcholine solution after exposed in 100 μg/mL isocarbophos solution (solvent: PBS buffer). In order to study this biosensor's detection effect, we need to compare the experiment concentration with the detection limit of the target organic phosphorous isocarbophos [34]. The I−V curves were recorded when gate voltage $V_g$ = 0 V before and after the addition of organic phosphorous, and graphene FET transfer curve characteristics were also recorded with a fixed bias voltage. We applied 0.8 V to the solution gate chamber, and this bias voltage $V_{ds}$ remained at 0.1 V. The I−V curves were recorded in the Figure 9. The Keithley 4200 instrument was kept in the transfer curve sweeping and recording mode. Thus, the transfer curves of each step of the experiment were recorded and drawn for comparison. We have recorded the transfer curves of the initial signal, the thiolation signal, the function signal and target signal. For the inhibition ratio calculation, the most important is the transfer

curves after adding the target organophosphorus isocarbophos [35]. In our experiment, the transfer curves were recorded when the target organophosphorus isocarbophos was added at the 1st minute, the 5th minute and the 10th minute, presenting in the Figure 10 below.

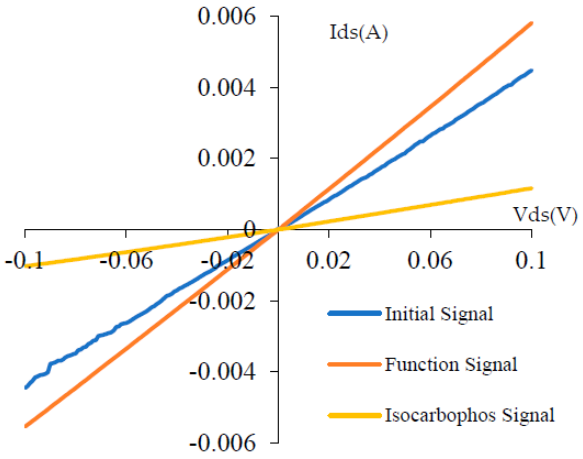


**Figure 9.** I−V curves corresponding to the initial signal, the AChE functionalizationsignal and the isocarbophos signal.

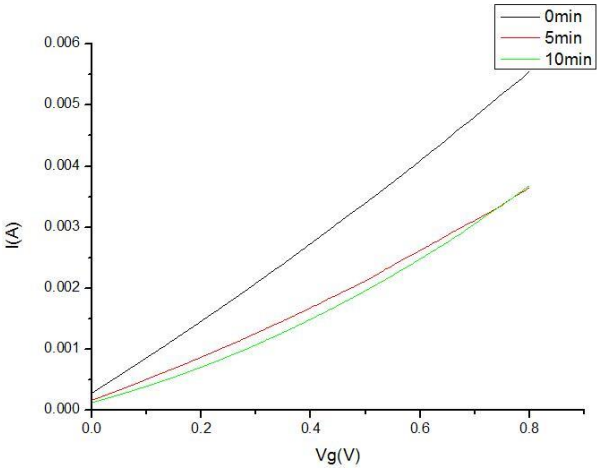


**Figure 10.** The transfer curves variation during the incubation time after adding our target organophosphorus isocarbophos sample.

We calculated the inhibition ratio over time, as shown in Figure 11:

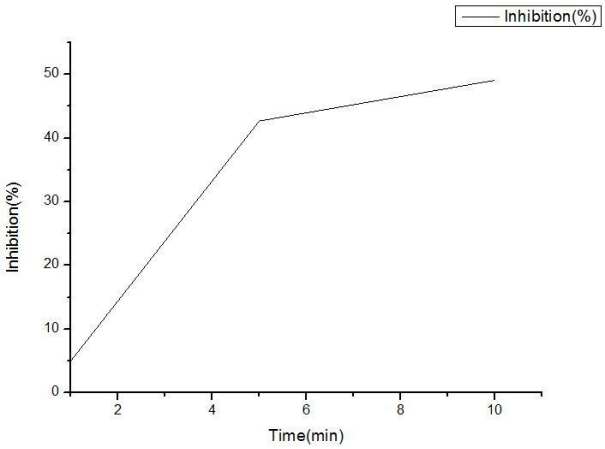


**Figure 11.** The inhibition ratio variation during the incubation time after adding our target organophosphorus isocarbophos sample.

To analyze our sensor's performance, we have conducted the transfer curves comparison and the inhibition curve comparison. The transfer curves in the 1st minute, the 5th minute, the 10th minute during the incubation of isocarbophos were recorded. It is indicated that as the incubation time increases, the transfer curve tends to be stable and the inhibition ratio is beginning to indicated saturation. The maximum inhibition ratio is maintained around the value below 50%.

However, our experiment has some limitations. We should have conducted measurement for more concentrations of the target isocarbophos and tested other kinds of organophosphorus. We will plan to replenish our measurement experiments and test more samples when the coronavirus crisis is over. Other organophosphorus compounds including malathion, chlorpyrifos and parathion samples will be collected and tested in our future experiments. Our research is of great significance to the pesticide residue detection and food safety field.

## 6. Conclusions

In summary, a graphene-based FET enzymatic sensor for organophosphorus detection has been developed, and the following sensing mechanism was demonstrated to explain the sensor signal. In the sensor fabrication and function process, the enzyme was fixed on the gold electrode by functionalization by using the linker MPA molecule. This sensor's many detection indexes to the target isocarbophos have been demonstrated. The biosensor result for detecting isocarbophos could be read from the I−V curves and transfer curves. Because the organic phosphorous molecules present a negative charge after attachment, the pesticide residue would cause an increase in holes with positive charge. In that case, the FET's bias current would increase due to the target molecules' attachment. Comparatively, the theoretical derivation could provide evidence for our experiment signal variation; the concentration of isocarbophos was detected to the limit of detection measurement. In our future research plan we would collect samples in more areas of China. We would add more experiments on the detection limits of organophosphorus measurement and test more kinds of organophosphorus including malathion, chlorpyrifos and parathion. The further detection work in future would strengthen and broaden research in the biosensor and food safety field.

**Author Contributions:** Writing—original draft preparation, J.Z.; investigation, M.F.; funding acquisition, G.L. All authors have read and agreed to the published version of the manuscript.

**Funding:** The Research start-up funding No.20045 of Fujian University of Technology.

**Informed Consent Statement:** We sincerely thank Zhu's former colleagues of Analytical Instrument Department of NACC, Guangzhou. They help us so much during the experiment.

**Data Availability Statement:** Some data and the information of this project are available online at http://www.fenxi.com.cn/index.html.

**Acknowledgments:** The authors are grateful to Jiang-han Chen and Guan-wen Zhang of NACC (Guangdong Province, China). The experiment was successfully completed with NACC's sincere help for preparing the organophosphorus sample.

**Conflicts of Interest:** The authors declare no conflict of interest for this paper.

## References

1. Kumar, J.S.; Murmu, N.C.; Kuila, T. Recent trends in the graphene-based sensors for the detection of hydrogen peroxide. *AIMS Mater. Sci.* **2018**, *5*, 422–466. [CrossRef]
2. Li, T.; Wang, B.; Du, G.; Zhang, B.; Zeng, Z.M. Electrical Performance of Multilayer $MoS_2$ Transistors on High-k $Al_2O_3$ Coated Si Substrates. *AIP Adv.* **2015**, *5*, 057102. [CrossRef]
3. Samnakay, R.; Jiang, C.; Rumyantsev, S.L.; Shur, M.S.; Balandin, A.A. Selective chemical vapor sensing with few-layer $MoS_2$ thin-film transistors: Comparison with graphene devices. *Appl. Phys. Lett.* **2015**, *106*, 023115. [CrossRef]
4. Gautam, M.; Jayatissa, A.H. Ammonia gas sensing behavior of graphene surface decorated with gold nanoparticles. *Solid-State Electron.* **2012**, *78*, 159–165. [CrossRef]

5. Sudibya, H.G.; He, Q.; Zhang, H.; Chen, P. Electrical Detection of Metal Ions Using Field-Effect Transistors Based on Micro patterned Reduced Graphene Oxide Films. *ACS Nano* **2011**, *5*, 1990–1994. [CrossRef]
6. Lerner, M.B.; Matsunaga, F.; Han, G.H.; Hong, S.J.; Xi, J.; Crook, A.; Perez-Aguilar, J.M.; Park, Y.W.; Saven, J.S.; Liu, R.; et al. Scalable Production of Highly Sensitive Nano-sensors Based on Graphene Functionalized with a Designed G Protein-Coupled Receptor. *Nano Lett.* **2014**, *14*, 2709–2714. [CrossRef]
7. Lü, M.; Li, J.; Yang, X.; Zhang, C.; Yang, J.; Hu, H.; Wang, X. Applications of graphene-based materials in environmental protection and detection. *Chin. Sci. Bull.* **2013**, *58*, 2698–2710. [CrossRef]
8. Cadore, A.; Mania, E.; Alencar, A.; Rezende, N.; de Oliveira, S.; Watanabe, K.; Taniguchi, T.; Chacham, H.; Campos, L.; Lacerda, R. Enhancing the response of NH3 graphene-sensors by using devices with different graphene-substrate distances. *Sensors Actuators B Chem.* **2018**, *266*, 438–446. [CrossRef]
9. Hess, L.H.; Hauf, M.V.; Seifert, M.; Speck, F.; Seyller, T.; Stutzmann, M.; Sharp, I.D.; Garrido, J.A. High-transconductance graphene solution-gated field effect transistors. *Appl. Phys. Lett.* **2011**, *99*, 033503. [CrossRef]
10. Rabchinskii, M.K.; Sysoev, V.V.; Glukhova, O.E.; Brzhezinskaya, M.; Stolyarova, D.Y.; Varezhnikov, A.S.; Solomatin, M.A.; Barkov, P.V.; Kirilenko, D.A.; Pavlov, S.I.; et al. Guiding Graphene Derivatization for the On-Chip Multisensor Arrays: From the Synthesis to the Theoretical Background. *Adv. Mater. Technol.* **2022**, *7*, 2101250. [CrossRef]
11. Chen, C.-H.; Chiang, C.-Y. Determination of the Highly Sensitive Carboxyl-Graphene Oxide-Based Planar Optical Waveguide Localized Surface Plasmon Resonance Biosensor. *Nanomaterials* **2022**, *12*, 2146. [CrossRef] [PubMed]
12. Wu, Z.; Li, F.; Li, X.; Yang, Y.; Huang, X.; Li, H. Direct Synthesis of $MoS_2$ Nanosheets in Reduced Graphene Oxide Nanoscroll for Enhanced Photodetection. *Nanomaterials* **2022**, *12*, 1581. [CrossRef] [PubMed]
13. Bhatt, V.D.; Joshi, S.; Becherer, M.; Lugli, P. Flexible, Low-Cost Sensor Based on Electrolyte Gated Carbon Nanotube Field Effect Transistor for Organo-Phosphate Detection. *Sensors* **2017**, *17*, 1147. [CrossRef]
14. Tuneli, A.; Bag, H.; Turker, A.R. Spectrophotometric Determination of Some Pesticides in Water Samples after Pre-concentration with Saccharomyces Cerevisiae Immobilized on Sepiolite. *Fresenius J. Anal. Chem.* **2001**, *371*, 1134–1138. [CrossRef] [PubMed]
15. Vallvey, L.F.C.; Deheidel, M.K.A.; Avidad, R. Determination of carbaryl in foods by solid-phase room-temperature phosphorimetry. *Anal. Bioanal. Chem.* **1998**, *362*, 307–312. [CrossRef]
16. Yao, W.; Gao, Z.; Cheng, Y. Quartz crystal microbalance for the detection of carbaryl using molecularly imprinted polymers as recognition element. *J. Sep. Sci.* **2009**, *32*, 3334–3339. [CrossRef]
17. Shang, Y.; Zhang, H.; Wang, X.; Wu, J. An Optical Olfactory Sensor Based on Porous Silicon Infiltrated with Room-Temperature Ionic Liquid Arrays. *Chem.—A Eur. J.* **2011**, *17*, 13400–13404. [CrossRef]
18. Chansi; Chaudhary, S.; Mani, A.; Bharadwaj, L.M.; Basu, T. A mobile app integrated portable Electrochemical sensor for rapid detection of Organophosphate pesticides in vegetable extract. *Mater. Lett.* **2022**, *309*, 131319. [CrossRef]
19. Rodrigues, A.; Barbieri, M.; Chino, M.; Manco, G.; Febbraio, F. A 3D Printable Adapter for Solid-state Fluorescence Measurements: The Case of an Immobilized Enzymatic Bioreceptor for Organophosphate Pesticides Detection. *Anal. Bioanal. Chem.* **2022**, *414*, 1999–2008. [CrossRef]
20. Mogha, N.K.; Sahu, V.; Sharma, M.; Sharma, R.K.; Masram, D.T. Biocompatible ZrO2- reduced graphene oxide immobilized AChE biosensor for chlorpyrifos detection. *Mater. Des.* **2016**, *111*, 312–320. [CrossRef]
21. Cui, H.F.; Wu, W.W.; Li, M.M.; Song, X.; Lv, Y.; Zhang, T.T. A Highly Stable Acetylcholinesterase Biosensor Based on Chitosan-$TiO_2$- Graphene Nanocomposites for Detection of Organophosphate pesticides. *Biosens. Bioelectron.* **2018**, *99*, 223–229. [CrossRef] [PubMed]
22. Mehta, J.; Vinayak, P.; Tuteja, S.K.; Chhabra, V.A.; Bhardwaj, N.; Paul, A.K.; Kim, K.-H.; Deep, A. Graphene modified screen printed immunosensor for highly sensitive detection of parathion. *Biosens. Bioelectron.* **2016**, *83*, 339–346. [CrossRef] [PubMed]
23. Brzhezinskaya, M.; Kapitanova, O.; Kononenko, O.; Koveshnikov, S.; Korepanov, V.; Roshchupkin, D. Large-scalable graphene oxide films with resistive switching for non-volatile memory applications. *J. Alloys Compd.* **2020**, *849*, 156699. [CrossRef]
24. Brzhezinskaya, M.; Kononenko, O.; Matveev, V.; Zotov, A.; Khodos, I.I.; Levashov, V.; Volkov, V.; Bozhko, S.I.; Chekmazov, S.V.; Roshchupkin, D. Engineering of Numerous Moiré Superlattices in Twisted Multilayer Graphene for Twistronics and Straintronics Applications. *ACS Nano* **2021**, *15*, 12358–12366. [CrossRef] [PubMed]
25. Hasani, A.; Dehsari, H.S.; Lafmejani, M.A.; Salehi, A.; Taromi, F.A.; Asadi, K.; Kim, S.Y. Ammonia-Sensing Using a Composite of Graphene Oxide and Conducting Polymer. *Phys. Status solidi (RRL)–Rapid Res. Lett.* **2018**, *12*, 1800037. [CrossRef]
26. Karimi, H.; Ahmadi, M.T.; Khosrowabadi, E.; Rahmani, R.; Saeidimanesh, M.; Ismail, R.; Naghib, S.D.; Akbari, E. Analytical prediction of liquid-gated graphene nanoscroll biosensor performance. *RSC Adv.* **2014**, *4*, 16153–16162. [CrossRef]
27. Petrone, N.; Meric, I.; Chari, T.; Shepard, K.L.; Hone, J. Graphene Field-Effect Transistors for Radio-Frequency Flexible Electronics. *IEEE J. Electron Devices Soc.* **2014**, *3*, 44–48. [CrossRef]
28. Petrone, N.; Meric, I.; Hone, J.; Shepard, K.L. Graphene Field-Effect Transistors with Gigahertz-Frequency Power Gain on Flexible Substrates. *Nano Lett.* **2012**, *13*, 121–125. [CrossRef] [PubMed]
29. Chu, K.L.; Wang, Z.B.; Zhou, J.J.; Jiang, H. Transport Properties in Monolayer-bilayer-monolayer Graphene Planar Junctions. *Chin. Phys. B* **2017**, *26*, 267202. [CrossRef]
30. Zhou, N.; Li, C.; Mo, R.; Zhang, P.; He, L.; Nie, F.; Su, W.; Liu, S.; Gao, J.; Shao, H.; et al. A Graphene/Enzyme-Based Electrochemical Sensor for Sensitive Detection of Organophosphorus Pesticides. *Surf. Rev. Lett.* **2015**, *23*, 1550103. [CrossRef]

31. Barik, A.M.; Deka, R.; Dutta, J.C. Carbon Nanotube-Based Dual-Gated Junction-less Field-Effect Transistor for Acetylcholine Detection. *IEEE Sens. J.* **2016**, *16*, 280–286. [CrossRef]
32. Kim, B.; Song, H.S.; Jin, H.J.; Park, E.J.; Lee, S.H.; Lee, B.Y.; Park, T.H.; Hong, S. Highly selective and sensitive detection of neurotransmitters using receptor-modified single-walled carbon nanotube sensors. *Nanotechnology* **2013**, *24*, 285501. [CrossRef] [PubMed]
33. Zhang, Y.; Arugula, M.A.; Wales, M.; Wild, J.; Simonian, A.L. A novel layer-by-layer assembled multi-enzyme/CNT biosensor for discriminative detection between organophosphorus and non-organophosphrus pesticides. *Biosens. Bioelectron.* **2015**, *67*, 287–295. [CrossRef]
34. Aduini, F.; Amine, A.; Moscone, D.; Palleschi, G. Biosensors Based on Cholinesterase Inhibition for Insecticides, Nerve agents and Aflatoxin B1 Detection (review). *Microchim. Acta* **2010**, *170*, 192–214.
35. Arduini, F.; Guidone, S.; Amine, A.; Palleschi, G.; Moscone, D. Acetylcholinesterase biosensor based on self-assembled monolayer-modified gold-screen printed electrodes for organophosphorus insecticide detection. *Sens. Actuators B Chem.* **2013**, *179*, 201–208. [CrossRef]